

Supplementary information for

The role of sp-hybridized boron atom in highly-efficient photocatalytic N₂ reduction activity of boron-doped triphenylene-graphdiyne

Yingcai Fan^{a,†}, Jingping Yu^{a, b,†}, Xiaohan Song^a, Yang Liu^a, Siyun Qi^a, Weifeng Li^a,
Mingwen Zhao*^{a, c}

^a *School of Physics, State Key Laboratory of Crystal Materials, Shandong University, Jinan, Shandong, China*

^b *School of Integrated Traditional Chinese and Western Medicine, Binzhou Medical University, Yantai, Shandong, China*

^c *School of Physics and Electrical Engineering, Kashgar University, Kashi, 844006, China*

† These authors contributed equally.

To whom correspondence should be addressed.

*Email: zmw@sdu.edu.cn (M. Zhao).

Text S1. The strategy of optical absorption calculation

The excitonic effects are considered in the framework of DFT-GW-BSE scheme¹⁻⁴ by VASP package to predict the accurate optical absorption of TP-GDY monolayer. A vacuum of 25 Å is used to minimize the interlayer coupling. The included conduction bands are 20 times of the valence bands, the energy cutoff for the response functions parameter was set to 200 eV and $15 \times 15 \times 1$ k-point meshes were used. All the valence bands and the same number of conduction bands are included in BSE calculation. All the parameters used in the GW-BSE calculations had been tested to ensure that the gaps are converged with the accuracy 0.01 eV⁵.

Text S2. The strategy of NAMD calculation

Our nonadiabatic molecular dynamics (NAMD) simulation for the photogenerated carriers transfer and e-h recombination were carried out by Hefei-NAMD code⁶, employing the quantum-classical decoherence-induced surface-hopping (DISH) technique⁷⁻⁹. The geometry optimization, electronic structure, and ab initio molecular dynamics (AIMD) trajectories are performed using the VASP with the PBE functional. After geometry optimization at 0 K, the systems are heated to 300 K by repeated velocity rescaling. Then, a 5 ps microcanonical AIMD trajectory is obtained with a 1 fs atomic time step. The corresponding wave function of the 5 ps AIMD trajectory were also generated. Due to the CBM and the VBM locate at the Γ -point, we select the Γ -point to conduct the NAMD simulations. For the simulation of the photogenerated carriers transfer, we selected 100 different initial configurations from the first 1 ps of AIMD trajectory. And the simulation results are based on averaging over the 20000 trajectories of these initial configurations for the last 4 ps. Next, for the simulation of the e-h recombination dynamics on a longer time scale, the 4 ps nonadiabatic Hamiltonians are iterated 250 times. These results are based on averaging over 50 random initial configurations and 2000 surface-hopping trajectories sampled for each initial structure.

The charge carrier lifetime in the ab initio NAMD simulations depends partly on the NAC which can be written as¹⁰:

$$d_{jk} = \left\langle \varphi_j \left| \frac{\partial}{\partial t} \right| \varphi_k \right\rangle = \frac{\langle \varphi_j | \nabla_R H | \varphi_k \rangle}{\varepsilon_k - \varepsilon_j} \dot{R}$$

where H is the electronic Hamiltonian, φ_j , φ_k , ε_k and ε_j are the wave functions and energies of electronic states k and j , and \dot{R} is velocity of the nuclei. Thus, the NAC depends on the energy difference $\varepsilon_k - \varepsilon_j$, the e-ph coupling matrix element $\langle \varphi_j | \nabla_R H | \varphi_k \rangle$ and the nuclear velocity term \dot{R} .

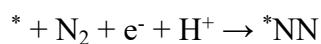
Text S3. The strategy of free energy calculation

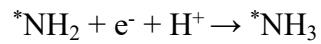
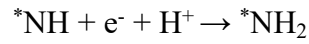
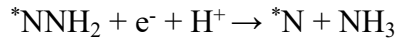
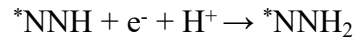
To compute the free energy change (ΔG) in the NRR and HER, we adopted the method developed by Nørskov *et al*, according to which the ΔG of an electrochemical reaction is computed as¹¹⁻¹⁴:

$$\Delta G = \Delta E + \Delta E_{ZPE} - T\Delta S + \Delta G_U$$

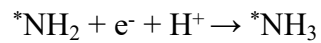
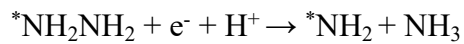
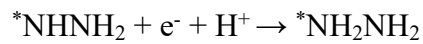
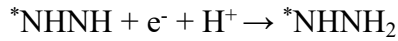
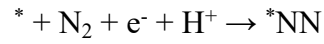
where ΔE , ΔE_{ZPE} and ΔS are the differences in DFT total energy, zero-point energy and entropy of the two states before and after reaction, respectively. T is the system temperature (298 K, in our work). ΔG_U represents the contribution of photogenerated electrode potential (U_e/U_h) to ΔG , which is relative to the normal hydrogen electrode (NHE). For each system, its E_{zpe} for each adsorbate and free molecules can be calculated by summing vibrational frequencies over all normal modes ν ($E_{zpe} = 1/2\sum\hbar\nu$), while the zero-point energy of adsorption sites is negligible. The entropies of the free molecules were taken from the standard tables in Physical Chemistry¹⁵. For those reactions involving the release of protons and electrons, the free energy of one pair of proton and electron ($H^+ + e^-$) was taken as $1/2G_{H_2}$. All the E_{ZPE} and S results and are shown in Table S2. The solvent effect was also considered in the work to simulate the intrinsic photocatalytic reaction as implemented in VASPsol^{16, 17}. The relative permittivity of the media was chosen as 78.4 referring to previous literatures^{18, 19}.

In the aqueous solution, the NRR process generally involves 6 electron reduction steps. For the distal pathway, the NRR process can be written as:

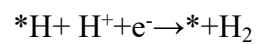
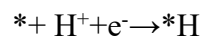




For the alternating pathway, the NRR process can be written as:



The HER process with two-electron pathways, including a fast proton/electron transfer step and a fast hydrogen release step, can be written as:



Text S4. Computational Method of MD simulations

MD simulations were carried out with Gromacs²⁰. The TP-GDY and B-doped TP-GDY molecules were solvated with TIP3P water molecules²¹, which were composed of 100 N₂ molecules. The Universal force field (UFF)²² were adopted to the TP-GDY and B-doped TP-GDY structures. The topology file of TP-GDY and B-doped TP-GDY were generated by the OBGMX program²³, which includes the bonded and nonbonded parameters from UFF, while the partial charges were obtained from Zheng et al.²⁴. Energy-minimization was first conducted with the steepest descent algorithm, followed by isothermal-isobaric equilibration at 298 K and 1 bar for 50 ps. Then, 50 ns MD runs were carried out under the NPT ensemble at 298 K and 1 bar, with Nose-Hoover thermostat and Parrinello-Rahman barostat controlling the system temperature and pressure, respectively.

Table S1. Cohesive energies of pristine TP-GDY monolayer and B_i@TP-GDY (i = 1, 5) monolayers.

Species	E_{coh} (eV)
TP-GDY	-7.879
B ₁ @TP-GDY	-7.781
B ₂ @TP-GDY	-7.784
B ₃ @TP-GDY	-7.793
B ₄ @TP-GDY	-7.782
B ₅ @TP-GDY	-7.784

Table S2. Calculated entropy and zero-point energy corrections of different adsorption species, where the * denotes the adsorption site. The ZPE and *TS* values of gaseous molecules and adsorbed molecules were obtained from the standard tables in Physical Chemistry and experimental values²⁵, respectively.

Species	ZPE (eV)	TS (eV)	ZPE-TS (eV)
H ₂	0.29	0.41	-0.12
H ₂ O	0.60	0.59	0.01
NH ₃	0.93	0.51	0.42
*NN	0.24	0.11	0.13
*NNH	0.52	0.15	0.37
*NNH ₂	0.85	0.12	0.73
*N	0.09	0.06	0.03
*NH	0.40	0.07	0.33
*NH ₂	0.76	0.07	0.69
*NH ₃	1.05	0.06	0.91
*NHNH	0.86	0.13	0.73
*NHNH ₂	1.21	0.12	1.09
*NH ₂ NH ₂	1.52	0.12	1.40
*H	0.23	0.01	0.22

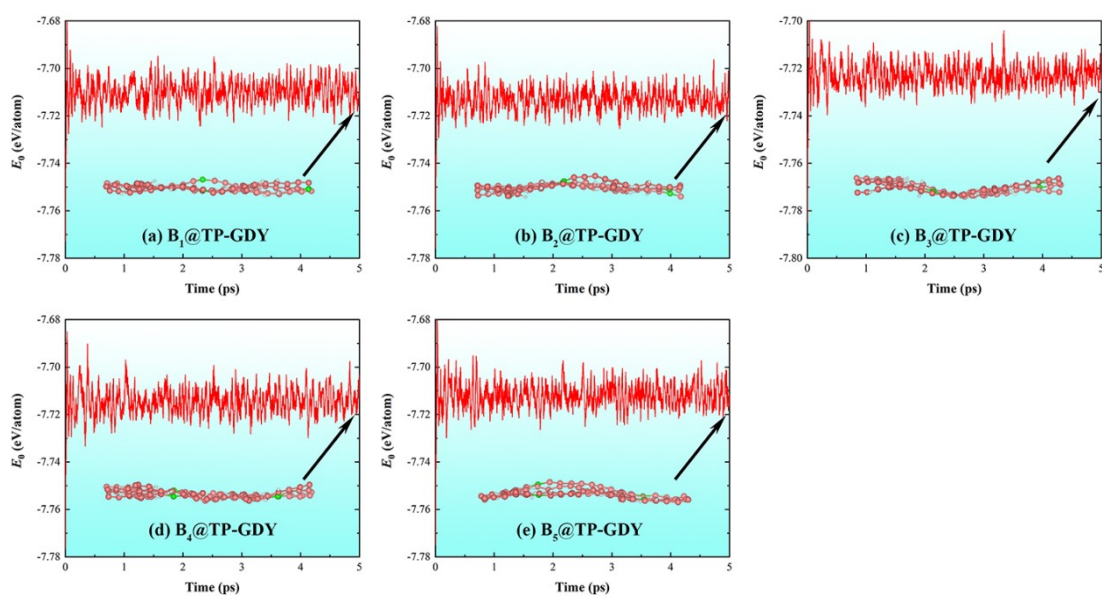


Figure S1. Evolution of total energies per atom of $B_i@TP-GDY$ monolayers ($i = 1, 5$) in the 2×2 supercells obtained from 5 ps AIMD simulations. The final conformations at $t = 5$ ps are shown in the insets.

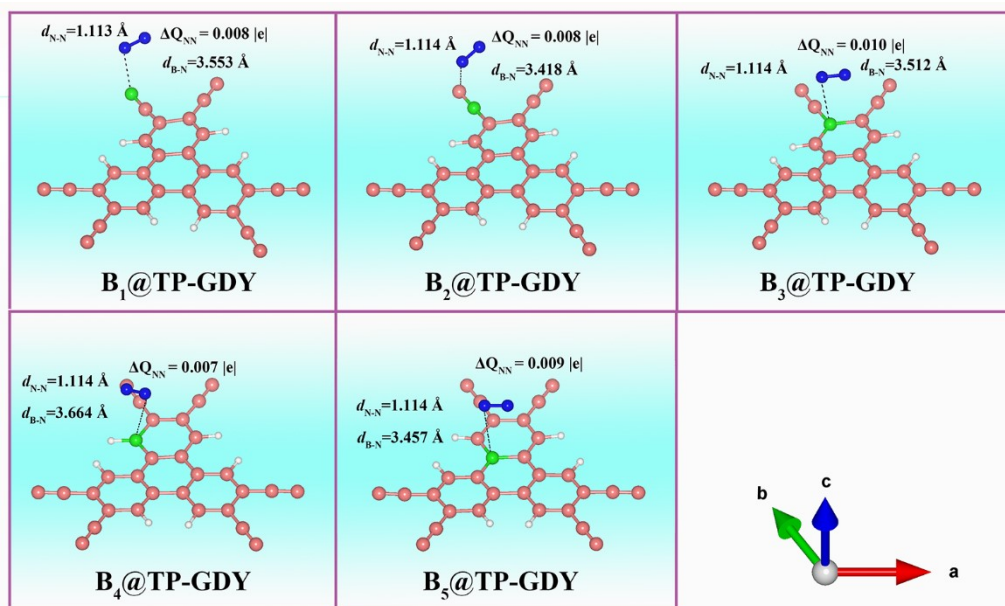


Figure S2. The N_2 adsorption configurations through the side-on patterns on these five $B_i@TP-GDY$ monolayers ($i = 1, 5$), respectively.

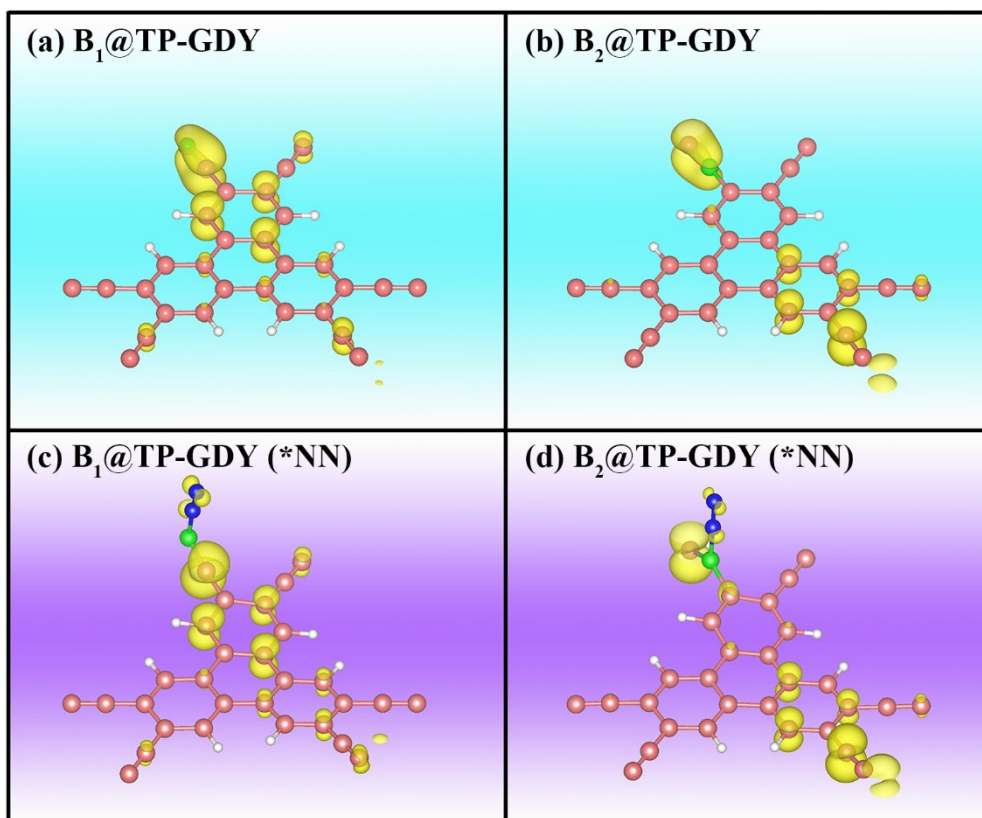


Figure S3. Spin-polarized densities before N_2 adsorption for the (a) $B_1@TP\text{-GDY}$ monolayer and (b) $B_2@GDY$ monolayer, respectively. Spin-polarized densities after N_2 adsorption for the (c) $B_1@TP\text{-GDY}$ monolayer and (d) $B_2@GDY$ monolayer, respectively.

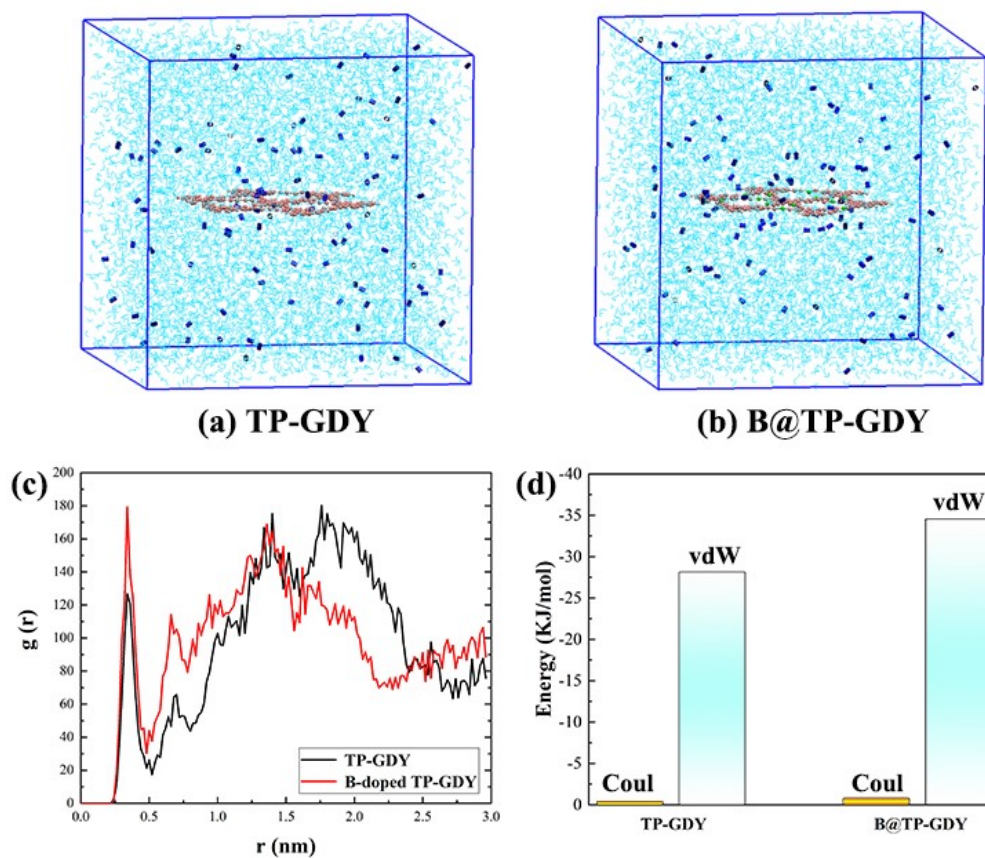


Figure S4. Molecular dynamics simulation snapshots of the (a) pristine TP-GDY monolayer and (b) B-doped TP-GDY monolayer. (c) Radial distribution function (RDF) of N_2 molecules around pristine TP-GDY and B-doped TP-GDY monolayers. (d) Coul and vdW interactions of TP-GDY and B-doped TP-GDY monolayers with the N_2 molecules.

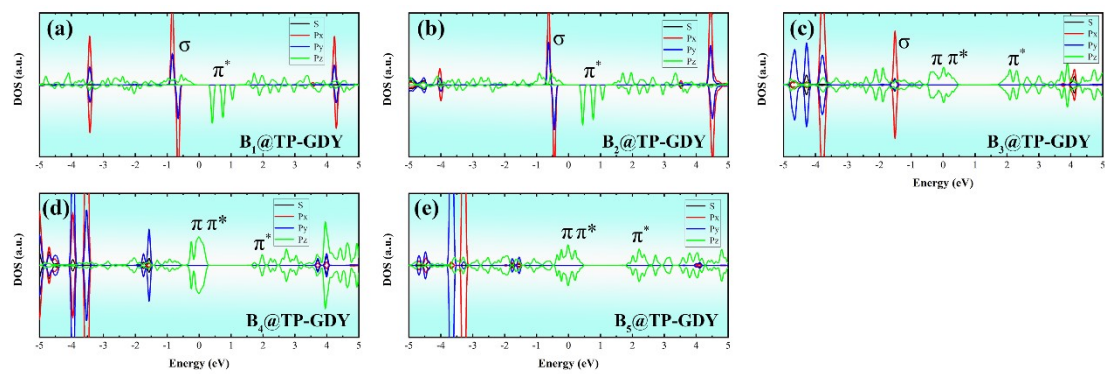


Figure S5. The partial density of states (PDOS) of B atoms in the $B_i@TP-GDY$ systems.

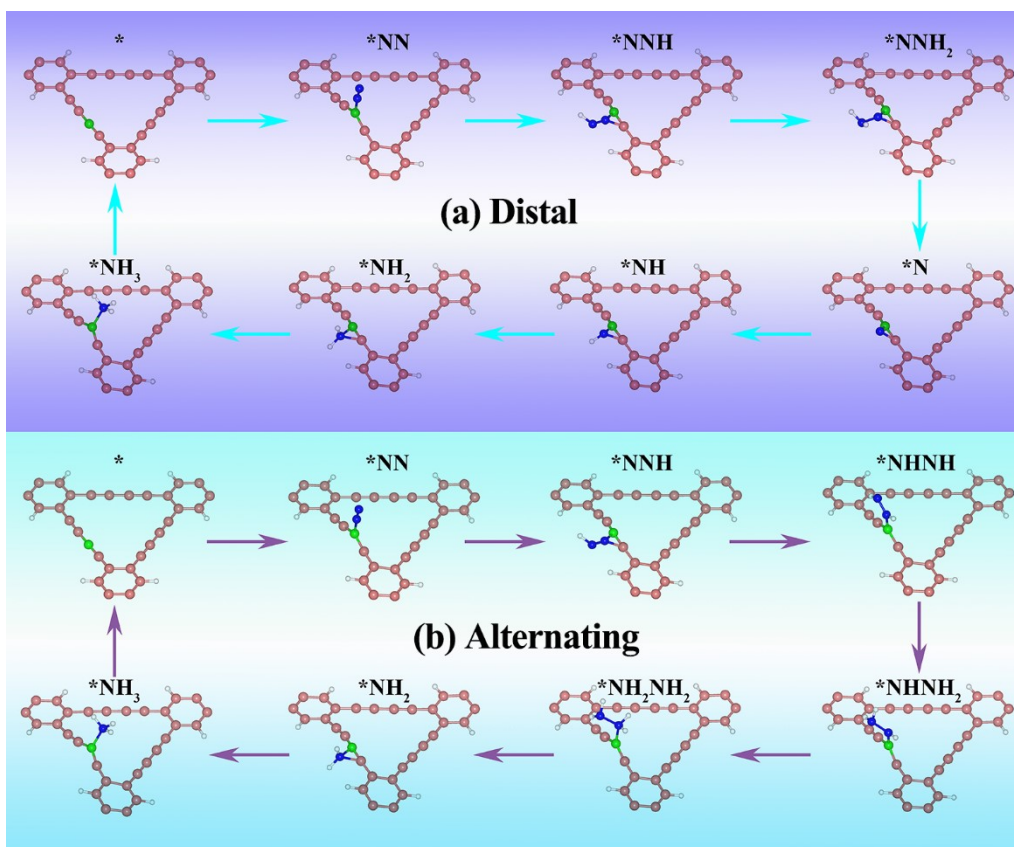


Figure S6. The structures of involved intermediates of $B_1@TP\text{-GDY}$ in the NRR processes along (a) distal and (b) alternating pathways, respectively.

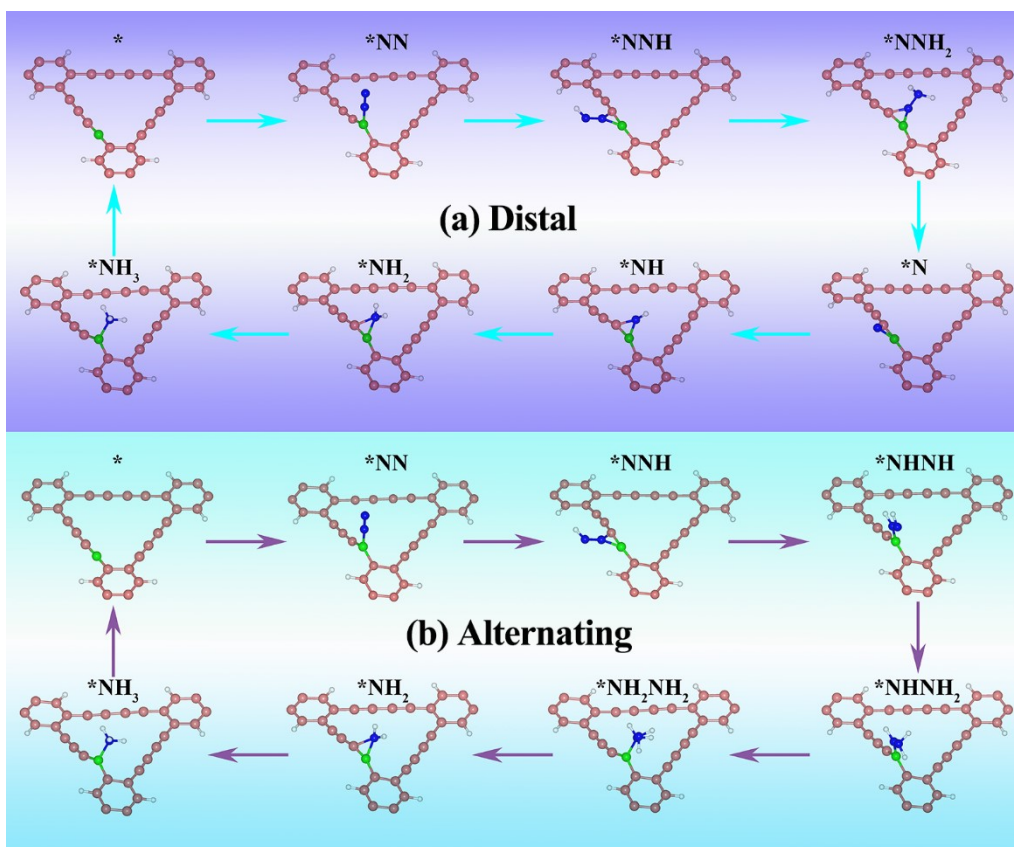


Figure S7. The structures of involved intermediates of $B_2@TP-GDY$ in the NRR processes along (a) distal and (b) alternating pathways, respectively.

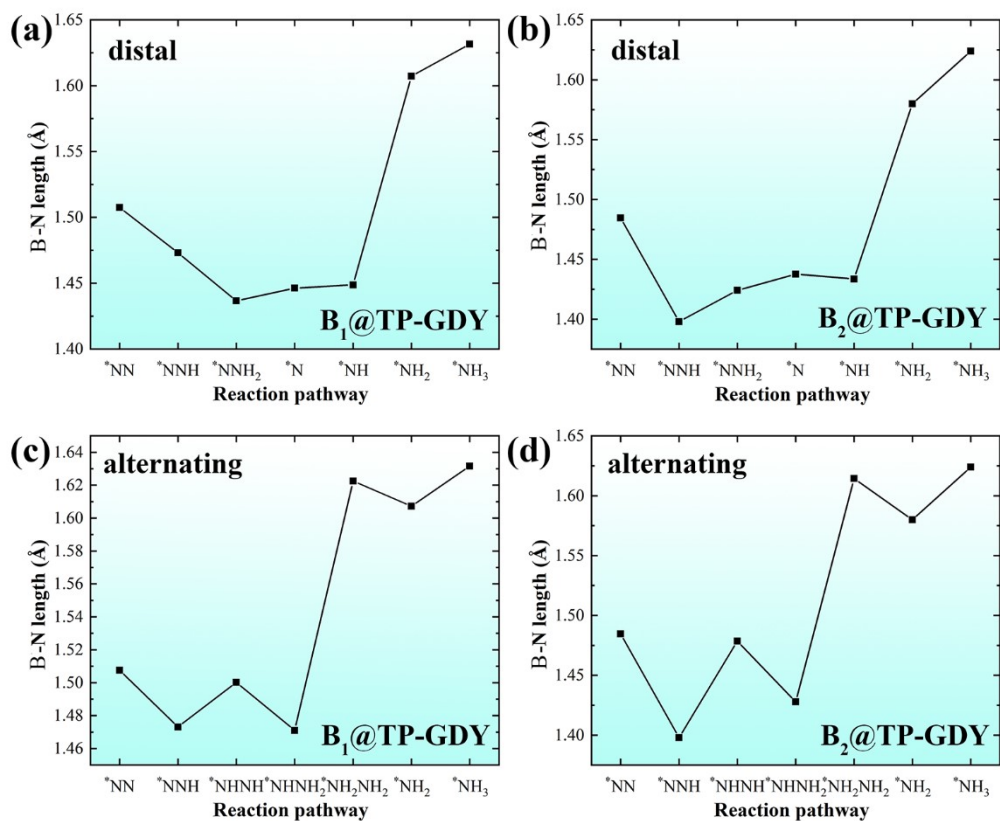


Figure S8. The B-N bond length for the (a) B₁@TP-GDY and (b) B₂@GDY monolayers along the distal pathway. The B-N bond length for the (c) B₁@TP-GDY and (d) B₂@GDY monolayers along the alternating pathway.

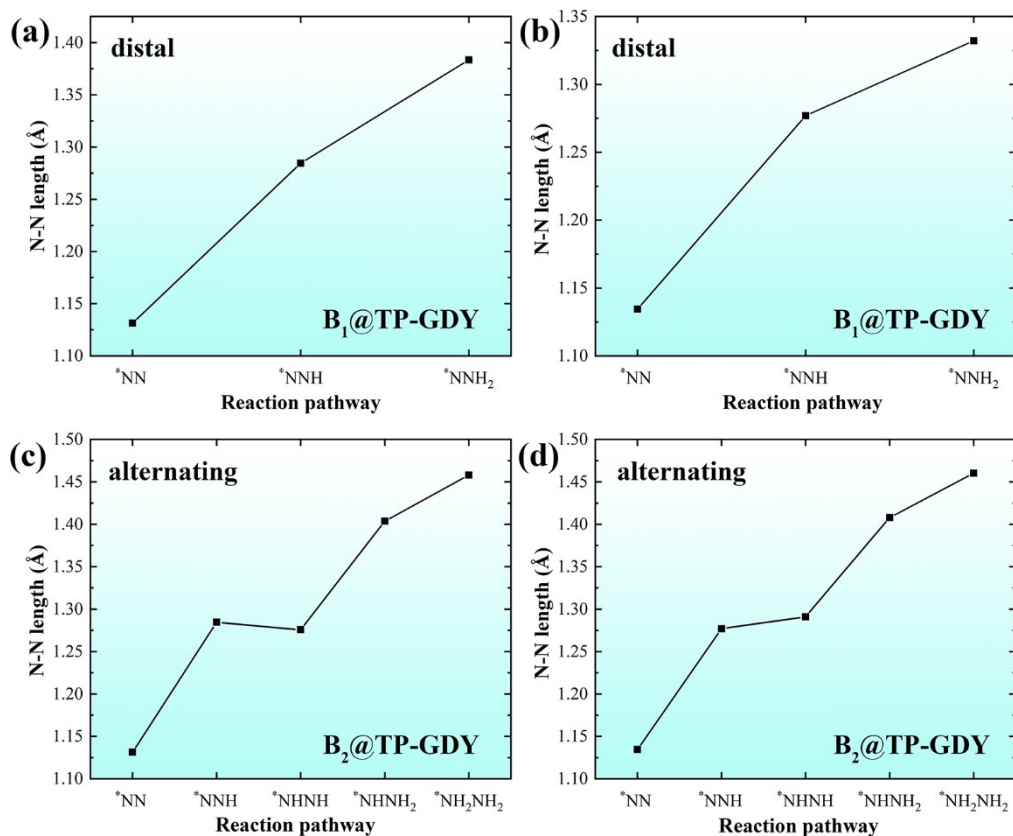


Figure S9. The N-N bond length for the (a) B₁@TP-GDY and (b) B₂@GDY monolayers along the distal pathway. The N-N bond length for the (c) B₁@TP-GDY and (d) B₂@GDY monolayers along the alternating pathway.

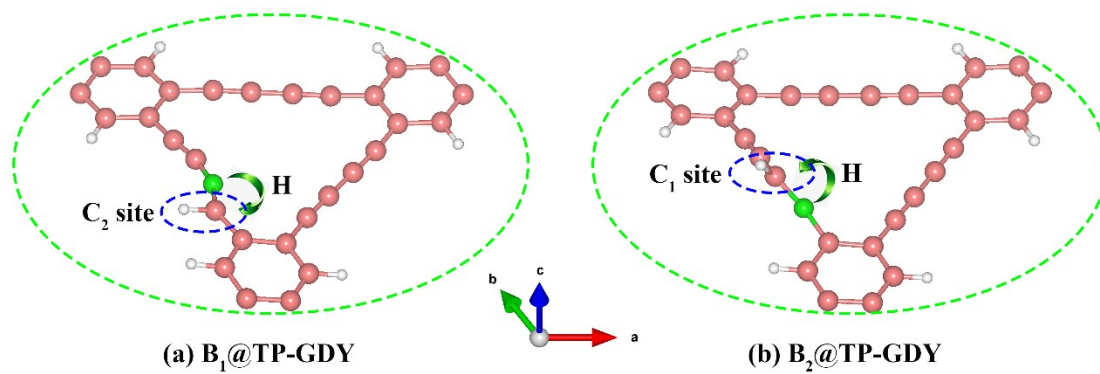


Figure S10. The adsorption and transfer of H atoms in the HER process for the (a) $B_1@TP-GDY$ and (b) $B_2@TP-GDY$ monolayers, respectively.

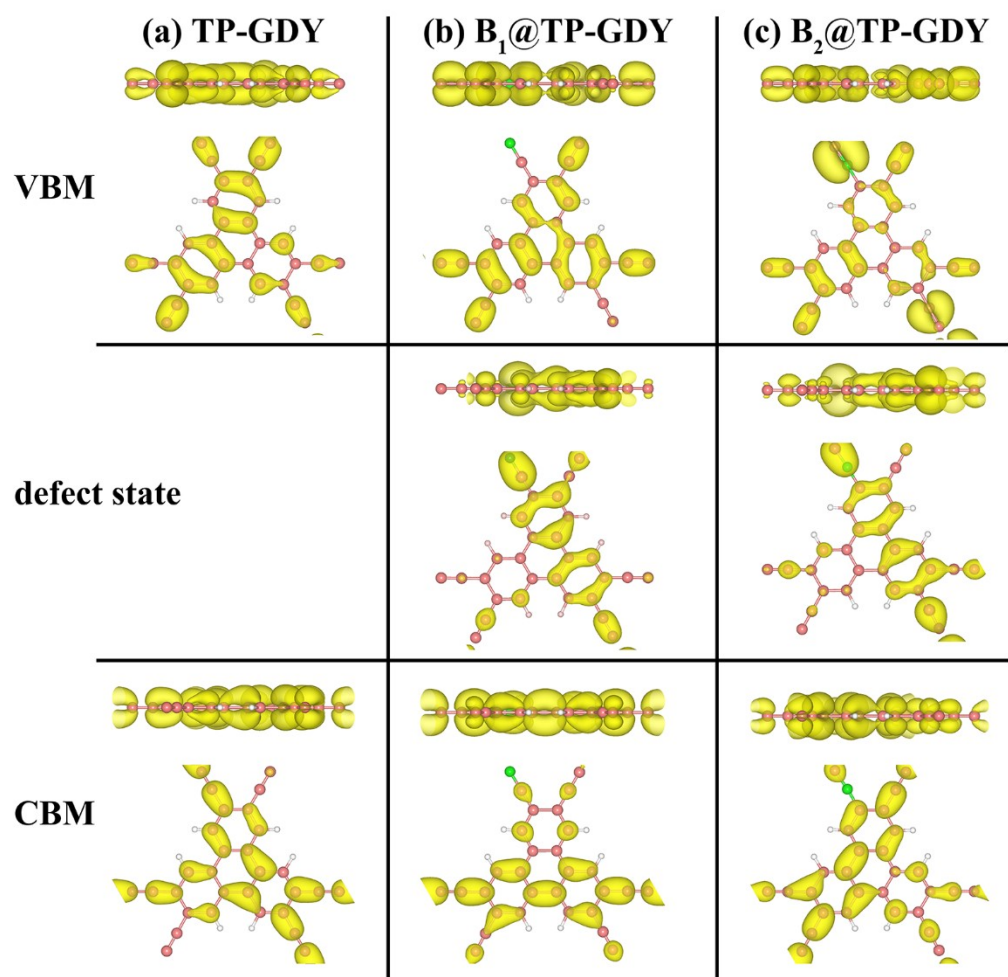


Figure S11. Side and top views of the charge densities of the VBM, CBM and defect states in (a) pristine TP-GDY monolayer, (b) B₁@TP-GDY monolayer and (c) B₂@TP-GDY monolayer.

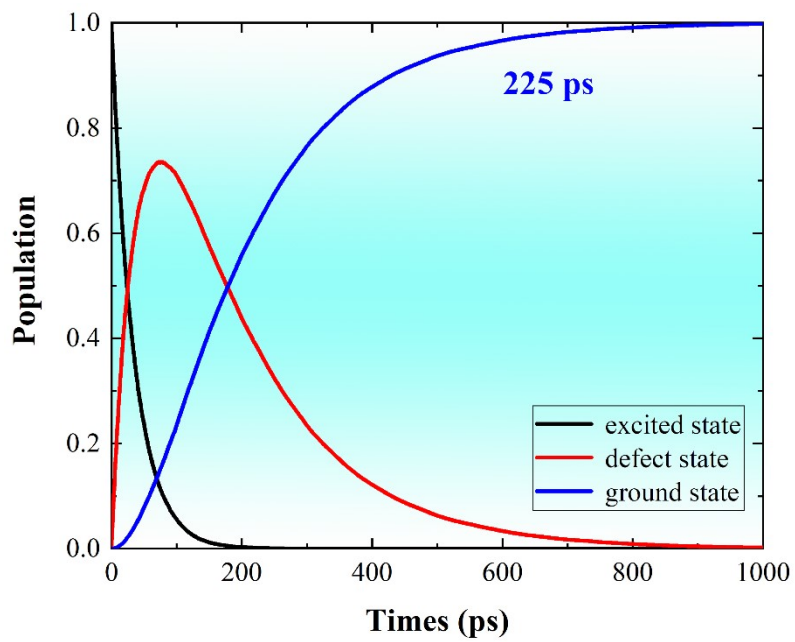


Figure S12. Populations of excited state, defect state and ground state in the B₂@TP-GDY monolayer.

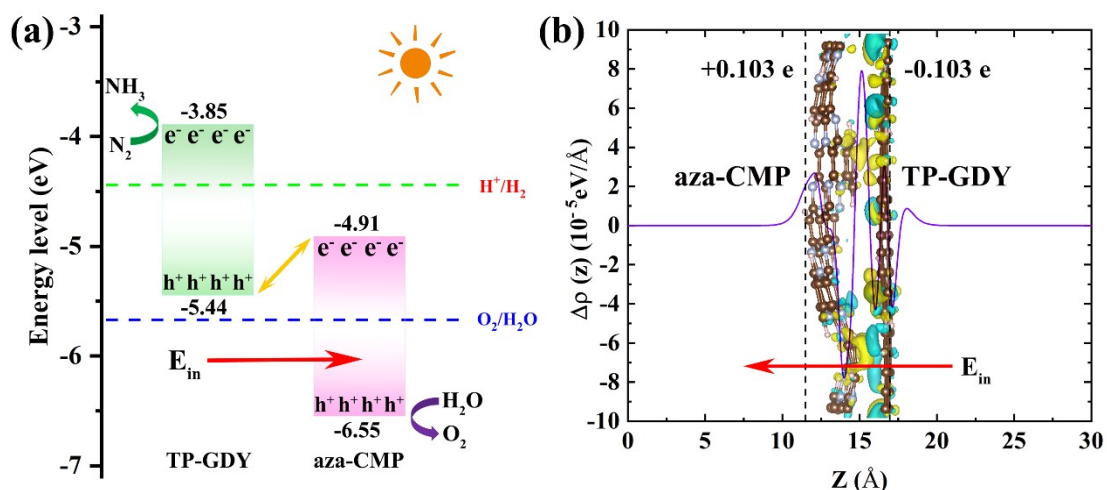


Figure S13. (a) Band alignment of $B_1@TP\text{-GDY}$ and aza-CMP in a Z-scheme heterostructure. (b) The averaged differential electron density along the z-direction of heterostructure. The supercells of this heterostructure has 2×2 TP-GDY monolayer on $\sqrt{3} \times \sqrt{3}$ aza-CMP with a lattice mismatch less than 3.1%. The isosurface of differential electron density with the isovalue of $0.0004|e|/\text{\AA}^3$ were plotted in the inset of this figure. The cyan and yellow regions denote electron depletion and deposition, respectively.

REFERENCES

1. M. S. Hybertsen and S. G. Louie, *Phys. Rev. B: Condens. Matter.*, 1986, **34**, 5390-5413.
2. M. Rohlfing and S. G. Louie, *Phys. Rev. Lett.*, 1998, **81**, 2312.
3. L. X. Benedict and E. L. Shirley, *Phys. Rev. Lett.*, 1998, **80**, 4514.
4. S. Albrecht and L. Reining, *Phys. Rev. Lett.*, 1998, **80**, 4510.
5. Z. Jiang, Z. Liu, Y. Li and W. Duan, *Phys. Rev. Lett.*, 2017, **118**, 266401.
6. Q. Zheng, W. Chu, C. Zhao, L. Zhang, H. Guo, Y. Wang, X. Jiang and J. Zhao, *WIREs: Comput. Mol. Sci.*, 2019, **9**, e1411.
7. C. F. Craig, W. R. Duncan and O. V. Prezhdo, *Phys. Rev. Lett.*, 2005, **95**, 163001.
8. H. M. Jaeger, S. Fischer and O. V. Prezhdo, *J. Chem. Phys.*, 2012, **137**, 22A545.
9. J. C. Tully, *J. Chem. Phys.*, 1990, **93**, 1061-1071.
10. K. G. Reeves, A. Schleife, A. A. Correa and Y. Kanai, *Nano Lett.*, 2015, **15**, 6429-6433.
11. J. K. Nørskov, J. Rossmeisl, A. Logadottir and L. Lindqvist, *J. Phys. Chem. B*, 2004, **108**, 17886-17892.
12. J. Greeley, T. F. Jaramillo, J. Bonde, I. B. Chorkendorff and J. K. Nørskov, *Nat. Mater.*, 2006, **5**, 909-913.
13. J. Rossmeisl, Z. W. Qu, H. Zhu, G. J. Kroes and J. K. Nørskov, *J. Electroanal. Chem.*, 2007, **607**, 83-89.
14. A. Valde's, Z.-W. Qu and G.-J. Kroes, *J. Phys. Chem. C*, 2008, **112**, 9872-9879.
15. E. Bianco, S. Butler, S. Jiang, O. D. Restrepo, W. Windl and J. E. Goldberger, *ACS Nano*, 2013, **7**, 4414-4421.
16. K. Mathew, R. Sundararaman, K. Letchworth-Weaver, T. A. Arias and R. G. Hennig, *J. Chem. Phys.*, 2014, **140**, 084106.
17. K. Letchworth-Weaver and T. A. Arias, *Phys. Rev. B*, 2012, **86**, 075140-075155.
18. Q. Zhang and A. Asthagiri, *Catal. Today*, 2019, **323**, 35-43.
19. A. J. Garza, A. T. Bell and M. Head-Gordon, *ACS Catal.*, 2018, **8**, 1490-1499.
20. M. J. Abraham, T. Murtola, R. Schulz, S. Páll, J. C. Smith, B. Hess and E.

- Lindahl, *SoftwareX*, 2015, **1-2**, 19-25.
21. W. L. Jorgensen, J. Chandrasekhar, J. D. Madura, R. W. Impey and M. L. Klein, *J. Chem. Phys.*, 1983, **79**, 926-935.
 22. A. K. Rappé, C. J. Casewit, K. S. Colwell, W. A. Goddard III and W. M. Skif, *J. Am. Chem. Soc.*, 1992, **114**, 10024–10035.
 23. G. Garberoglio, *J. Comput. Chem.*, 2012, **33**, 2204-2208.
 24. C. Zheng and C. Zhong, *J. Phys. Chem. C*, 2010, **114**, 9945–9951.
 25. C. T. Campbell and J. R. Sellers, *J. Am. Chem. Soc.*, 2012, **134**, 18109-18115.